Science of the Total Environment 936 (2024) 173423

Contents lists available at ScienceDirect

Science of the Total Environment

journal homepage: www.elsevier.com/locate/scitotenv

Microbial consortium involved in ferromanganese and francolite biomineralization in an anchialine environment (Zinzulùsa Cave, Castro, Italy)

Adriano Guido [a,*], Matteo Calcagnile [b], Adelfia Talà [b], Salvatore Maurizio Tredici [c], Genuario Belmonte [b], Pietro Alifano [c]

[a] Department of Biology, Ecology and Earth Sciences, University of Calabria, Rende, Cosenza, Italy
[b] Department of Biological and Environmental Sciences and Technologies, University of Salento, Lecce, Italy
[c] Department of Experimental Medicine, University of Salento, Lecce, Italy

HIGHLIGHTS

- Geomicrobiological characterization of Zinzulùsa cave, an anchialine setting, was performed.
- Water chemistry, oligotrophic and aphotic conditions promoted peculiar biomineralization.
- Ferromanganese and francolite mineralization were mediated by a specific microbial consortium.
- "*Ca. Manganitrophus noduliformans*" was molecularly identified in the microbial consortium.
- SEM images revealed traces of fossilized microorganisms resembling "cable bacteria".

GRAPHICAL ABSTRACT

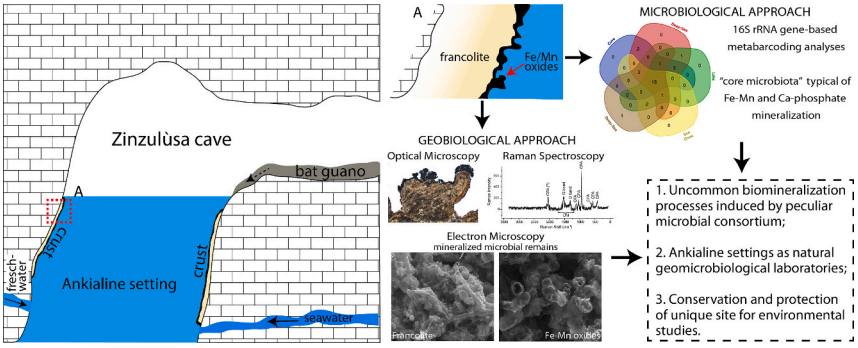

ARTICLE INFO

Editor: Daniel Alessi

Keywords:
Anchialine cave
Biogeochemical cycles
Ca-phosphate
Vernadite
Hematite
Microbial biomineralization
Iron and manganese oxidation and reduction

ABSTRACT

Tidally-influenced subterranean settings represent natural geomicrobiological laboratories, relatively unexplored, that facilitate the investigation of new biomineralization processes. The unusual water chemistry of Zinzulùsa Cave and its oligotrophic and aphotic conditions have allowed the development of a unique ecosystem in which complex bacterial activities induce rare biomineralization processes. A diversified microbial community develops on centimeter-thick crusts that form in the submerged part of the cave. The crusts are formed of Ca-phosphate minerals, mostly carbonate-fluoroapatite (francolite), covered by a black crust, few microns in thickness, composed of ferromanganiferous oxides (hematite and vernadite). Diffuse coccoidal and filamentous bacteria and amorphous organic matter are mixed with the minerals. The micromorphologies and comparative 16S rRNA gene-based metabarcoding analyses identify a "core microbiota" also common to other natural environments characterized by Fe—Mn and Ca-phosphate mineralization. The microbiota is characterized by nitrifying, sulfide/sulfur/thiosulfate-oxidizing and sulfate/thiosulfate/sulfur-reducing bacteria. In addition, manganese-oxidizing bacteria include the recently described "*Ca.* Manganitrophus noduliformans" and an

* Corresponding author.
E-mail addresses: aguido@unical.it (A. Guido), matteo.calcagnile@unisalento.it (M. Calcagnile), adelfia.tala@unisalento.it (A. Talà), maurizio.tredici@unisalento.it (S.M. Tredici), genuario.belmonte@unisalento.it (G. Belmonte), pietro.alifano@unisalento.it (P. Alifano).

https://doi.org/10.1016/j.scitotenv.2024.173423
Received 4 March 2024; Received in revised form 3 May 2024; Accepted 19 May 2024
Available online 24 May 2024

abundance of bacteria belonging to the Planctomycetes-Verrucomicrobia-Chlamydiae (PVC) superphylum, as well as Haliangiales (fruiting body-forming bacteria) and Hyphomicrobiales (stalked and budding bacteria) that are known to produce extracellular polymers that trap iron and manganese oxides. 16S rRNA gene metabarcoding analysis showed the presence of bacteria able to utilize many organic P substrates, including *Ramlibacter*, and SEM images revealed traces of fossilized microorganisms resembling "cable bacteria", which may play a role in Ca-phosphate biomineralization. Overall, the data indicate biomineralization processes induced by microbial metabolic activities for both ferromanganiferous oxide and francolite components of these crusts.

1. Introduction

Mineral nucleation related to biotic activities is generally termed biomineralization. The processes and the products linked to biomineralization have attracted attention in a wide range of research fields, from geobiology to the bioengineering, during recent decades. Many of the best known and most studied biomineralization processes are connected to the production of carbonate minerals. However, biochemical influences on the nucleation process are not always well-defined or easily recognizable, and a uniform terminology is still a matter of debate (Perry et al., 2007; Altermann et al., 2009; Dupraz et al., 2009; Anbu et al., 2016; Riding and Virgone, 2020). In general, three different mechanisms can be recognized in the production of carbonate biominerals: 'biologically controlled', 'biologically influenced' and 'biologically induced'. Biologically controlled mineralization is regulated by cellular activities which modulate solubility, supersaturation, nucleation and crystal growth (Lowenstam and Weiner, 1989; Mann, 1983, 2001; Weiner and Dove, 2003; Benzerara et al., 2011; Phillips et al., 2013; Anbu et al., 2016; Riding and Virgone, 2020). In this process, the organisms directly control mineral nucleation and growth at specific locations within or on the cellules. In biologically influenced mineralization mineral precipitation may be triggered by the presence of cell surface organic matter, such as extracellular polymeric substances associated with biofilms (Dupraz et al., 2009; Benzerara et al., 2011; Phillips et al., 2013; Anbu et al., 2016). In biologically induced mineralization, precipitation of minerals is a localized response to the production of metabolic byproducts (e.g. OH^-, $HCO3^-$) which chemically modify the microenvironment (Lowenstam and Weiner, 1989; Stocks-Fischer et al., 1999; Frankel and Bazylinski, 2003; Dupraz et al., 2009; De Muynck et al., 2010; Phillips et al., 2013; Riding and Virgone, 2020).

Diverse microbial metabolic pathways, including photosynthesis, ammonification, denitrification, ureolysis, and methane oxidation, have been shown to influence redox conditions and lead to carbonate precipitation in a range of natural environments (Fortin et al., 1997; Douglas and Beveridge, 1998; Zhu and Dittrich, 2016). Bacterial surfaces, including cell walls and extracellular polymeric substances (EPS), have also been reported to act as important sites for carbonate mineral nucleation and growth (Douglas and Beveridge, 1998; Bains et al., 2015).

Mineralization unconnected to any biological or organic control is regarded as abiotic precipitation. In this case, mineralization is related to the carbonate saturation state, influenced by the physicochemical properties of the environment and climatic factors (Stumm and Morgan, 1996; Zeebe, 2012; Riding and Virgone, 2020).

Many studies of mineralization that involve the direct or indirect role of organisms have focused primarily on open marine environments. Relatively few investigations have focused on subterranean environments, and in particular submerged anchialine caves. Extreme and confined conditions in submerged caves can be ideal for microbial growth, including heterotrophic and phototrophic bacteria, which have also been described from terrestrial caves (Cubbon, 1976), such as both aerobic (Abdelahad, 1989; Jones, 1995) and anaerobic limestone and dolostone caves (Sarbu et al., 1996; Mattison et al., 1998). Cave geochemistry, physico-chemical conditions, and mineralogy can significantly impact the microbiome, and microbe-mineral interactions may further play a significant role in the formation and characteristics of biomineralized speleothems (Zepeda-Mendoza et al., 2016).

The majority of speleothems in terrestrial caves have been found to be composed of calcium carbonate polymorphs such as calcite, vaterite, and aragonite (Ronholm et al., 2014; Demény et al., 2016; García et al., 2016). Speleothem growth through calcite precipitation has long been viewed as an essentially abiogenic process (Kendall and Broughton, 1978; Broughton, 1983a, 1983b, 1983c). However, mineral deposits that are difficult to explain by inorganic chemical-physical processes raise the possibility of microbial activity in caves (Jones, 2001). Numerous studies have investigated microbial biofilms associated with chemical conditions on the surfaces of subaerial cave walls (Cunningham et al., 1995; Holmes et al., 2001; Adetutu et al., 2012; Pacton et al., 2013; Barton et al., 2014; Wu et al., 2015; Northup et al., 2003; Macalady et al., 2007; Chen et al., 2009; Rusznyak et al., 2012; Zepeda-Mendoza et al., 2016). In contrast, relatively few recent studies have focused on the role of microorganisms, especially bacteria, in the formation of authigenic marine cave minerals, especially carbonate (Sanfilippo et al., 2015; Gischler et al., 2017a, 2017b; Guido et al., 2013, 2014, 2016, 2017a, 2017b, 2019, 2022). This research area remains relatively unexplored, especially with regard to biomineralization processes that may be involved in non-carbonate mineral phases such as iron and magnesium oxides and apatite.

There is increasing evidence that microbial processes play a critical role in the formation and remodeling of ferromanganese deposits (crusts and nodules) in aphotic cave environments, including iron and manganese oxidation and reduction, and precipitation of iron or manganese oxides. Although iron oxide minerals can be formed through both biotic and abiotic processes, manganese oxides, hydroxides and oxyhydroxides are usually associated with the presence of Mn-oxidizing microorganisms. Since abiotic manganese oxidation is thermodynamically unfavorable, even in the presence of oxygen (Johnson et al., 2013; Luther, 2010), Mn-oxidizing microorganisms may increase the rate of this process by several orders of magnitude (Geszvain et al., 2012; Tebo et al., 2005; Tebo et al., 2010). In cave systems, several Mn-oxidizing microorganisms may be involved in this process, especially heterotrophic bacteria and fungi (Carmichael and Bräuer, 2015). Furthermore, some Hyphomicrobiales bacteria, such as *Hyphomicrobium* and *Pedomicrobium*, can be involved in the biogenesis of ferromanganiferous crusts through the production of extracellular polymers that act as matrices for the deposition of iron and/or manganese oxides (Cox and Sly, 1997; Gebers and Beese, 1988).

On the other hand, anaerobic respiratory reduction of manganese oxides may contribute to the remodeling of ferromanganese deposits (Myers and Nealson, 1988; Lovley and Phillips, 1988). Importantly, it was considered highly unlikely that chemolithoautotrophic oxidation of Mn could support microbial growth and the formation of ferromanganese deposits, until the discovery, in tap water, of a bacterial coculture that formed nodules using chemolithoautotrophic manganese oxidation (Yu and Leadbetter, 2020). The principal member of this coculture was named "*Candidatus* Manganitrophus noduliformans", belonging to a distinct lineage of the phylum Nitrospirota (Yu et al., 2022). Limited information is also available concerning the involvement of microorganisms and their metabolic processes on apatite mineralization in cave systems. This includes evidence that the precipitation of phosphate minerals within a few centimeters of the sediment/water interface can be directly related to microbial activity (Bailey et al., 2013; Cosmidis

et al., 2013b; Crosby and Bailey, 2012; Goldhammer et al., 2010; Krajewski et al., 1994; Schulz and Schulz, 2005), although questions remain concerning this process. Several models (Cosmidis et al., 2013a, 2013b), discussed below, include: 1) organic matter remineralization; 2) iron redox pumping; and 3) polyphosphate metabolism.

Within this framework, we have investigated dark crusts that form in the anchialine submerged part of the Zinzulùsa Cave (southern Italy). This anchialine environment is a tidally-influenced subterranean water body, within crevicular and cavernous terrain, that extends inland beyond the limit of seawater penetration. The oligotrophic and aphotic conditions of this cave habitat create a unique system for the investigation of complex prokaryotic interactions involved in unusual biomineralization processes in cryptic environments.

Low pH is commonly associated with haloclines in anchialine caves, likely due to CO_2 production by microbial oxidation of particulate organic matter. At haloclines, the combination of fresh- and salt-water, both saturated with dissolved $CaCO_3$, can create low-pH conditions that results in aggressive limestone dissolution. Although diverse species, as well as higher taxonomic categories, have been described from anchialine systems in the last 20–30 years, knowledge regarding prokaryotes is much more limited. Similarly, although exploration of these flooded caves has advanced greatly, biological studies, particularly with regard to interactions between living species and the environment, have only just began. Some anchialine species, such as those of the copepod genus *Expansophria*, represent biological and evolutionary links between anchialine and deep-sea species that have been forced to migrate to keep space with tectonic uplift and glacio-eustatic sea-level change. This can only occur in the presence of a vertical continuum of suitable habitats in both time and space (Iliffe and Alvarez, 2018). Whereas biological and ecological studies of submarine caves are at a pioneering stage, elucidating the role of microbiota in the modification and/or creation of substrates remains at an explorative level (Talà et al., 2021; Guido et al., 2013, 2022).

We used a multidisciplinary approach, coupling petrographic, geochemical, biogeochemical and 16S rRNA gene metabarcoding analyses, to: (a) describe micro- and macrotextures of the Zinzulùsa crusts; (b) characterize their mineral composition; (c) study the relationship between organic material and mineral phases; (d) detect microbial communities and their possible roles in biomineralization processes; and (e) compare the processes and products investigated in the natural environment with similar data obtained in laboratory.

2. Location, geology and geomorphology of the Zinzulùsa Cave

In this study we focused on the geology, morphology and microbiology of the Zinzulùsa Cave. The coastline of the Otranto Channel (Salento peninsula, Italy), is marked by steep cliffs and karst caves that open at both submerged and emerged parts of the coast. Some of these have sulfur springs (D'Angeli et al., 2019; D'Angeli et al., 2017; Margiotta and Negri, 2008; Calò and Tinelli, 1995). The area is characterized by Cretaceous carbonates locally covered by Cenozoic successions. The Cretaceous (Calcare di Altamura) consists of compact fossiliferous carbonates, occasionally associated with dolomitic limestones. Oligocene carbonates, which crop out in the coastal area between Castro Marina and Porto Miggiano, consist of bioclastic and organogenic limestones (Calcari di Castro) (Pomar et al., 2014). These are overlain by the Plio-Pleistocene Calcareniti del Salento), made of coarse brown-yellowish calcarenites and compact detrital-organogenic limestones.

The Zinzulùsa Cave is located on the Castro coast of the Apulian peninsula, in south-eastern Italy (40.011905 N, 18.431212 E) (Fig. 1). It has a karstic origin and can be subdivided in three distinct parts. The first part develops in Eocene limestone and extends from the entrance to the Cripta hall. It is characterized numerous stalactites and stalagmites. The second part results from erosion of Cretaceous carbonates. It is characterized by fewer stalactites and stalagmites, and extends from the Cripta hall to the large hall called the Duomo. The third part, the most confined part, ~25 m from the Duomo, is characterized by the presence of the Cocito, an anchialine brackish water environment of submerged cavities down to 12 m below the sea level, extending for about 160 m (Pesce, 2001; Onorato, 1996; Talà et al., 2021). Biological studies of this anchialine environment described three endemic organisms: *Higginsia ciccaresei* (sponge), *Psyllocamptus monachus* (harpacticoid), and *Stygocyclopia badinoi* (calanoid) (Pesce and Galassi, 1987; Ciccarese and Pesce, 1999; Pesce, 2003; Belmonte, 2022). The submerged part of the Cocito walls is covered by black crusts which are the focus of our geomicrobiological study (Fig. 2).

Previous study revealed the presence of a complex microbial community on the bottom (S) and on the walls (WB) of this cave, in

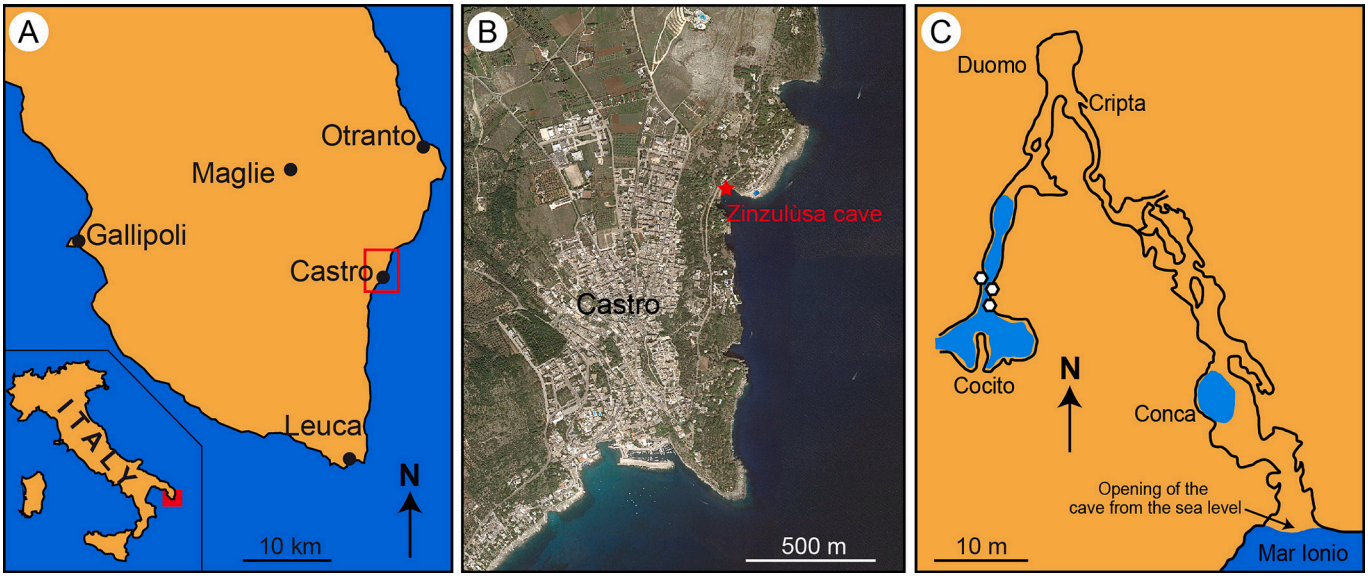

Fig. 1. Location of the study site. (A) Location of Castro, southern Italy. (B) Google Earth photo showing the location of the Zinzulùsa Cave. (C) Outline map of the Zinzulùsa Cave based on the original August 1958 relief map of A. Lazzari and V. Sticchi (Lazzari, 1966), modified in Talà et al. (2021). White polygons indicate the locations of the black crusts studied on the rocky walls in the Cocito area. Dark blue indicates the Ionian Sea near the opening of the cave; light blue indicates the anchialine water inside the cave.

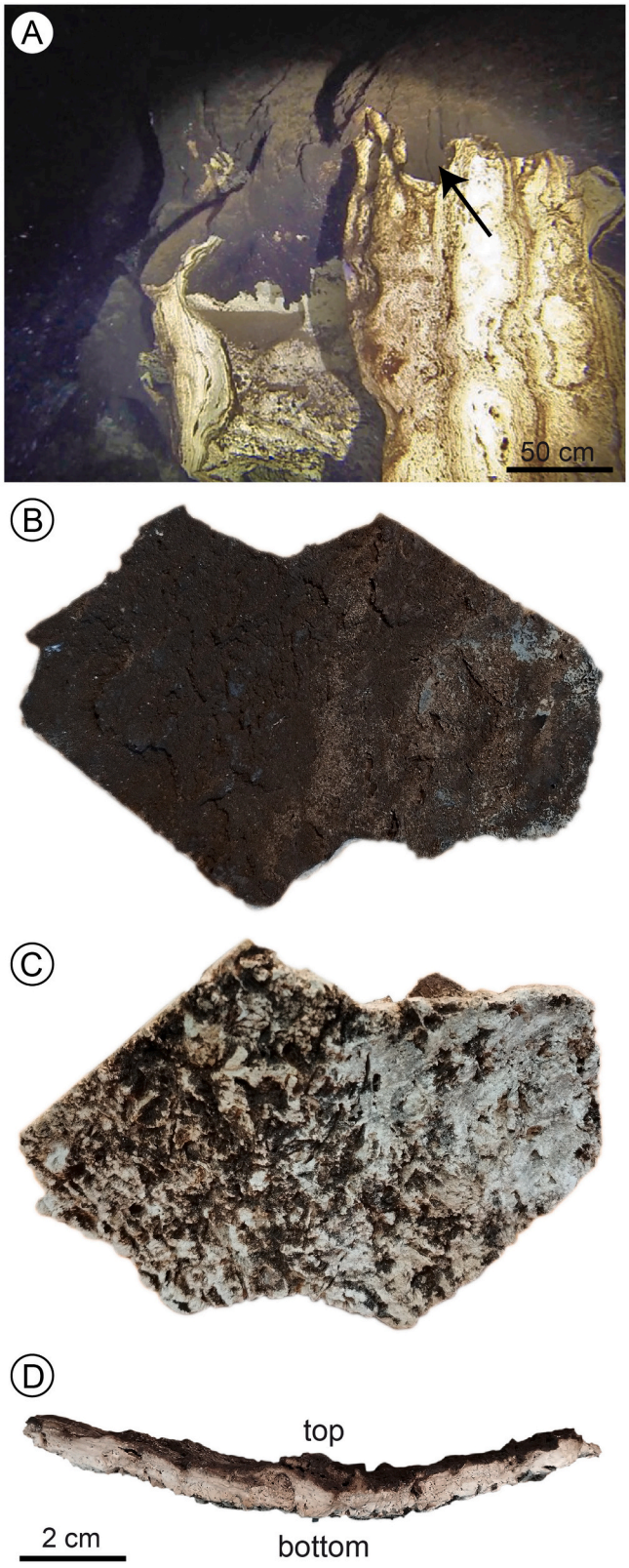

Fig. 2. (A) Submerged part of the Cocito area with continuous black crusts covering the walls (photograph of R. Onorato). (B) Upper part (top) of a crust characterized by a dark mineralized patina. (C) Lower part (bottom) of the same crust detached from the substrate; this crust was already partially detached from the substrate prior to sampling and was starting to be covered of the same dark patina that forms in the upper part. (D) Transverse section showing the thin dark cover of the upper surface and the yellow to white the internal part.

particular on centimeter thick black crusts that form at a depth of 3–4 m (for details of S and WB samples see table 1 of Talà et al., 2021). The presence of microbes does not automatically imply that they played a role in the formation of the surrounding minerals because they may simply have been entombed during mineral precipitation (Polyak and Cokendolpher, 1992; Forti, 2001). Here, by combining microscopical, geochemical and metabarcoding, we aim to precisely constrain the role of microbes in the crust formation in this cave.

3. Materials and methods

3.1. Morphological and mineralogical characterization

Fresh samples of three crusts were thin sectioned, analyzed by optical microscopy, mineralogically characterized using X-ray powder diffraction (XRPD) analyses, and chemically analyzed using electron microscopy and Raman spectrometry.

3.1.1. Optical and electron microscopy

Uncovered thin sections (48 × 28 mm) and polished slabs were studied with an optical microscope (Zeiss Axioplan II Imaging), up to 40× magnification, to detect the main textures. The same thin sections were also examined through fluorescence to reveal the distribution of the organic matter. Fluorescence was induced by an Hg vapor lamp linked to a Zeiss Axioplan II imaging microscope equipped with high performance wide band pass filters (BP 436/10 nm/LP 470 nm for green light; BP 450–490 nm/LP 520 nm for yellow light).

Following transmitted light and epifluorescence characterization, the thin sections and fresh fragments were used for Scanning Electron Microscope (SEM) observations and microanalyses by Energy Dispersive X-Ray Spectroscopy (EDS) and Electron Probe Micro Analyzer (EMPA). They were polished and gently etched (0.05 % HCl, 1 min). The SEM is a FEI Philips ESEM-FEG Quanta 200F, operating at 15 kV and with a working distance between 10 and 15 μm. The EMPA is a JEOL - JXA 8230, operating set is: 15 kV, probe current 10 nA, working distance 11 mm, take-off angle 40°, live time 50 s.

3.1.2. X-ray powder diffraction (XRPD) analyses

Three powdered samples were analyzed by XRPD to determine the main mineralogical phases of the crusts. Briefly, about 100 mg of sample was ground with an agate pestle and mortar to produce a homogeneous powder with an average grain size of few microns. Each powdered sample was gently mounted in the central hole of a cylindrical zero background sample holder, made of oriented Si monocrystalline wafer. The XRPD patterns were scanned with a BrukerD8 Advance diffractometer, with CuKα radiation in the range 3°– 66° 2θ, with steps of 0.02° 2θ and step-times of 1 s/step, at the University of Calabria (Italy). Semiquantitative mineralogical analysis of the bulk rock was carried out on random powders, measuring peak areas using the WINFIT computer program (Krumm, 1999), according to the procedure proposed by Cavalcante et al. (2023) and Perri et al. (2024). The percentage of the mineral phase was determined using the strongest reflection of each mineral.

3.1.3. Raman spectroscopy

Raman Spectroscopy was used to investigate the components of the crusts and to discriminate between their organic or inorganic nature. This technique, coupled with epifluorescence observations, allowed us to recognize the presence of organic compounds and to distinguish biomineralized components, of putative microbial origin, from abiotic ones. Micro-Raman analyses were performed on polished slabs and thin sections using a Thermo Fisher DXR Raman microscope (Waltham, MA, USA), equipped with OMNICxi Raman Imaging software 1.0, an objective of 50×, a grating of 900 ln/mm (full width at half maximum, FWHM), and an electron multiplying charge-coupled device (EMCCD). The 532 nm line (solid state laser) was used at an incident power output

ranging from 1.8 to 7 mW. The spatial resolution of the laser beam was about 3–5 μm. The acquisition time of the spectra varied from 5 to 40 s. Data were collected in the 50–3360 cm − 1 range to capture the first and second order Raman bands. The measurements were made on randomly oriented grains, with a fixed orientation of the polarized laser beam.

3.2. Gene metabarcoding characterization

3.2.1. Source of 16S rRNA gene metabarcoding data from ferromanganiferous crusts and taxonomy assignment by Illumina BaseSpace pipeline and "RDP database"

The taxonomy was assigned using Illumina BaseSpace (https://basespace.illumina.com) and RefSeq RDP 16S v3 May 2018 DADA2 32 bp database, as previously described (Talà et al., 2021). The fastq files, used as input for this study, were previously obtained from four samples taken from a rock wall with blackish manganese oxide concretions in the Zinzulùsa Cave that were available from the SRA database (PRJNA1026609) (Talà et al., 2021). To compare the bacterial community identified in the blackish concretion of the Zinzulùsa Cave with other communities identified in Fe—Mn crusts, fastq sequence files were downloaded from ENA (paired sequences) to reprocess the sequences together using the same database and algorithms. The accession numbers for the projects containing the selected files are PRJDB6715 and PRJNA638744 (Kato et al., 2018; Bergo et al., 2021). The fastq sequence files included in this analysis were selected based on diversity of geographical sampling sites and the depth of sampling, in order to search for microbial taxa specifically associated with the Fe—Mn crusts. In particular, the bioinformatic analysis was carried out on: (i) twenty-one samples (Fe—Mn crust) from two deep-sea sites in Pacific Ocean: eleven samples Takuyo-Daigo Seamount (tagged "DSC-G" in our analysis) and ten samples Takuyo-Daisan Seamount (tagged "DSC-S" in our analysis) in the Northern hemisphere (Kato et al., 2018); (ii) five samples (Fe—Mn crust, Fe-Mn-encrusted coral skeleton) from a deep-sea site (Southwestern Atlantic Ocean: Rio Grande Rise) in the Southern hemisphere (Bergo et al., 2021) (tagged "SC" in our analysis); (iii) four samples (Fe—Mn crust) from the submerged part of Zinzulùsa Cave in the Mediterranean Sea (Talà et al., 2021) (tagged "ZC" in our analysis). The analyzed sequences were obtained by amplifying either the V3-V4 region (for ZC and SC samples) (Talà et al., 2021; Bergo et al., 2021) or the V4 region alone (for DSC-G and DSC-S samples) of the 16S rRNA gene (Kato et al., 2018). The geographical coordinates, sampling depth, sample type and accession numbers of the sequences used are reported in Table S1.

3.2.2. Analysis of 16S rRNA gene metabarcoding data

16S rRNA gene metabarcoding data were analyzed at the genus level. Raw data were represented as the number of reads per bacterial genus. Relative abundance was calculated by dividing the number of reads for each genus by the total number of reads in that sample. Subsequently, the data were subjected to filtering, where only genera with a relative abundance >0.1 % in at least 10 out of 30 samples were considered. This filtering resulted in 133 bacterial genera, which were used to generate a heatmap (http://www.heatmapper.ca/expression/). The heatmap represented the relative abundance of bacterial genera in each sample and grouped the samples based on similarity in relative abundance patterns. The heatmap parameters were set as follows: Scale Type: rows; Clustering Method: Average Linkage; Distance Measurement Method: Euclidean; Apply Clustering To: Rows; Show Dendrogram; Rows. In addition, the abundance values of the 133 genera were analyzed using PAST (Hammer and Harper, 2001) to generate boxplots displaying the mean and standard deviation.

3.2.3. Python-based sequences analysis for identification of specific microbial taxa

Mothur (version 1.43.0) (Schloss et al., 2009) was used to generate a fasta file from paired-end fastq files using the 'make.file' and 'make.contigs' commands. Files generated from the DSC-G, DSC-S, SC and ZC datasets were used to perform the Python-based analysis, along with sequences from 16S metabarcoding of four sediment samples collected from the Zinzulùsa Cave (Zinzulùsa sediment, ZS1, ZS2, ZS3 and ZS4). Python 3.10.12 was utilized to execute the code 'Identity_filtering90.py', which was designed to filter sequences based on an identity threshold of >90 % compared to the 16S rRNA gene sequences selected as queries (Table S2). In this step, three sequences of "Ca. Manganitrophus" genus and three sequences of *Ramlibacter* genus were used as queries. A second code, 'identity_calculation.py' was employed to calculate the identity value between a set of reference sequences (Manganitrophus_references and Ramlibacter_references fasta files; DOI: https://doi.org/10.5281/zenodo.10575873) and the sequences filtered in the preceding step. The sequences with an identity value >95 % were selected. The EzBioCloud 16S-based identification tool was used to classify the sequences taxonomically (Yoon et al., 2017).

Finally, Vsearch version 2.23.0 (Rognes et al., 2016) was used to cluster the sequences using an identity threshold of 97 %. The representative sequence from each cluster was used as input to generate a phylogenetic tree. Sequence alignment was performed using the Muscle algorithm via MegaX (Kumar et al., 2018). The phylogenetic tree was generated using MegaX (Kumar et al., 2018) with the maximum likelihood algorithm, and then analyzed using iTOL (Letunic and Bork, 2021). All sequences and scripts used in this analysis are public available at DOI:https://doi.org/10.5281/zenodo.10575873

4. Results

4.1. Morphology and microstructures

The analyzed crusts have tabular morphologies and are characterized by irregular dendritic external surface and variable thickness (from few millimeters to one centimeters) (Fig. 2). The crusts are black on the external surface and white on the side attached to the walls. Those partially detached from the substrate and exposed to the environmental condition of the cave show the beginning of deposition of dark patina on the detached surface, similar to that on the surficial part (Fig. 2).

The internal part is composed of dense homogeneous dark-brown material, passing gradually to friable and porous white material in the most internal part (Fig. 3A). The yellow area between the dark-brown and white shows an intermediate consistency. Fine brownish laminae are observable on the transition from the dark-brown to the white part (Fig. 3A).

The dark cover of the crusts is formed by very fine minerals organized in clots mixed with mucilaginous amorphous material (Fig. 4A,C). Under UV-excitation the amorphous substance shows bright fluorescence denoting organic nature (Fig. 4B,D). Thin sections observed in transmitted light reveal a dense clotted peloidal texture in the dark-brown material below the external dark cover, while the yellow and white areas, that appear black in transmitted light, consist of fine aphanitic material (Fig. 3B). Both materials show bright fluorescence under UV-excitation, revealing, also in this case, high organic matter content strictly related to the minerals (Fig. 3D,F).

SEM observation indicates a close connection between bacterial (and possibly fungal) remains and the mineral phases. The external dark cover shows fine minerals closely intermingled with filaments and very small spherulites (Figs. 5 and 6). The filaments appear smooth, woven or segmented on the external surface, and often have empty internal tubules (Fig. 5). Their diameter is about or <1 μm, and they may show external incrustation (Fig. 5B,C) or, in other cases, well preserved ultrastructure (Fig. 5B,D,F), that suggest their attribution to specific bacterial taxa, thereby linking the micromorphological data with the 16S rRNA gene metabarcoding data, and/or with bibliographic data (discussed in the next sections). Amorphous material is strictly limited to fine minerals and filaments (Fig. 5C,D). In particular, SEM images (Fig. 5B) show the presence of well-preserved structures consisting of

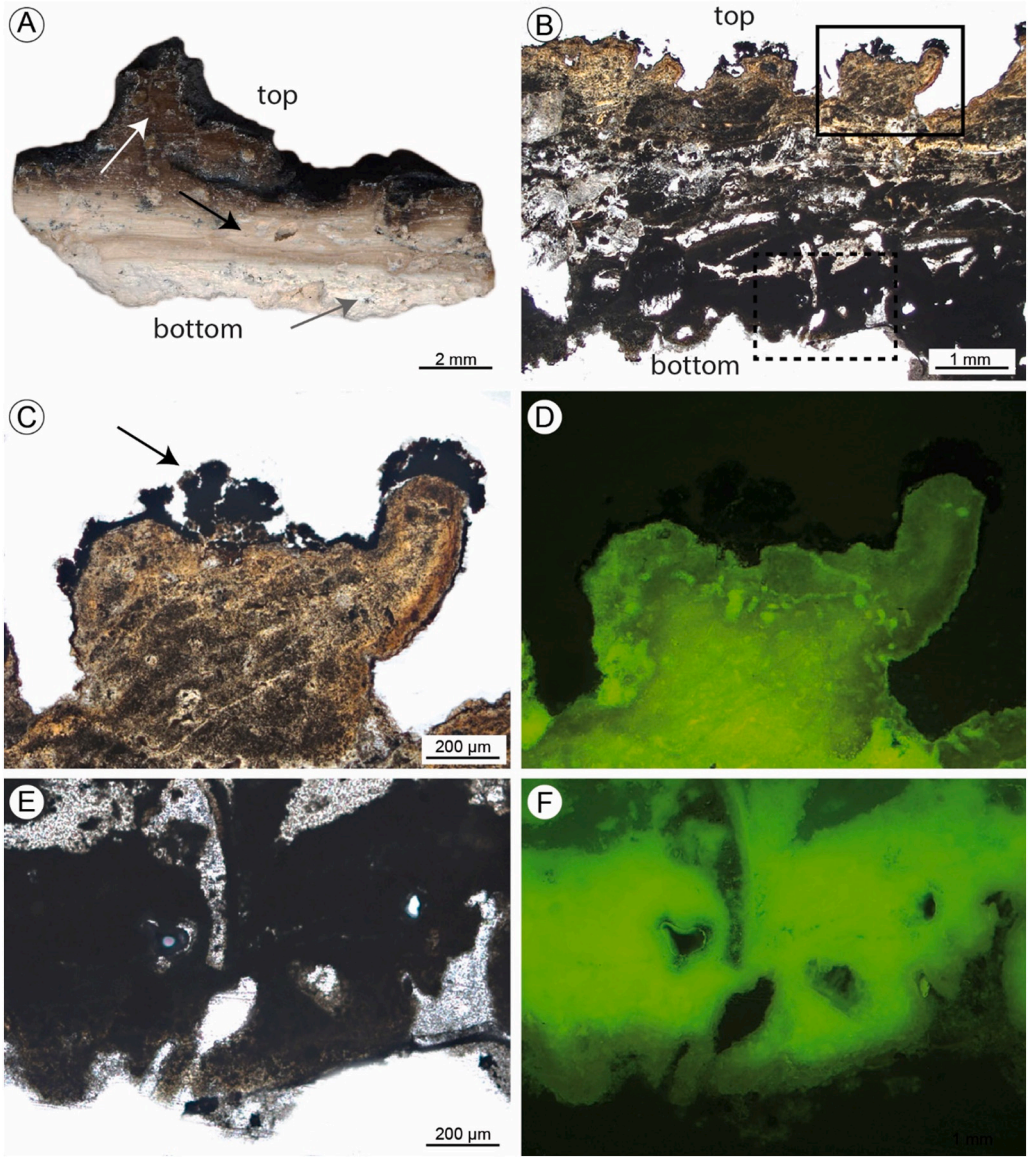

Fig. 3. (A) Close-up photo of a small polisched fragment collected transversely to the crust surface; note the color variation from dark-brown (white arrow) to yellow (black arrow) to white (grey arrow). (B) Thin section photo showing the general morphologies of the internal part of the crust; rectangles represent the details shown in C (continuous line) and E (dashed line). (C-D) Transmitted light (left) and UV-epifluorescence (right) photos of the upper part of the crusts just below the dark patina of the external surface (arrow). (E-F) Transmitted light (left) and UV-epifluorescence (right) photos of the most internal part of the crusts. Note the homogeneous high epifluorescence, denoting high organic matter content, strictly connected with the mineral forming the crust.

filaments with longitudinal strings (about 20–40 nm wide) running along the filaments (dashed black arrows in Fig. 5B), resembling those of "cable" bacteria (Meysman, 2018).

Very small spherulites show mineralized surface and empty internal cavities (Fig. 6A,B). The overall diameter is lesser than 2 µm. The walls of the spherules have varied thicknesses of 50 to 100 nm and are composed of anhedral minerals, a few nanometers in size. The internal wall surface of the spherules appears smooth in comparison to the external part. Mineralization of coccoid-like bacteria may account for these micromorphologies.

The internal part of the crusts, observed on fresh fragments, shows homogeneous micromorphologies, independent of color (dark-brown, yellow and white). It consists of very fine rod-like particles without clearly defined crystalline form (Fig. 6C,D). These are engulfed in amorphous material which is less abundant in the most internal part, originally attached to the cave wall.

4.2. Mineralogical composition

The main mineralogical phases of the crusts were recognized via XRPD analyses. The most intense reflections are attributable to a francolite ($(Ca_{10-a-b}Na_aMg_b(PO_4)_{6-x}(CO_3)_{x-yz}(CO_3,F)_y(SO_4)_zF_2)$ crystalline phase (Fig. 7). This phase accounts for almost 97 % of the total crystalline material, making it difficult to detect minor reflections attributable to accessory crystals. Nonetheless, among these, iron oxides (hematite, Fe_2O_3) and mancanese oxides (vernadite, $Mn(OH)_4$) are recognized.

EDS microanalyses indicates the chemical composition and confirms the crystalline phases of the crusts detected by XRPD analyses. The external dark cover mainly reveals the presence of Mn and Fe, compatible with the presence of iron and manganiferous oxides (hematite and vernadite oxides) detected by XRPD analyses; while the internal part is composed mainly of Ca, P, F, Na, Mg and S, consistent with the francolite, or carbonatefluoroapatite (CFA), crystalline phase

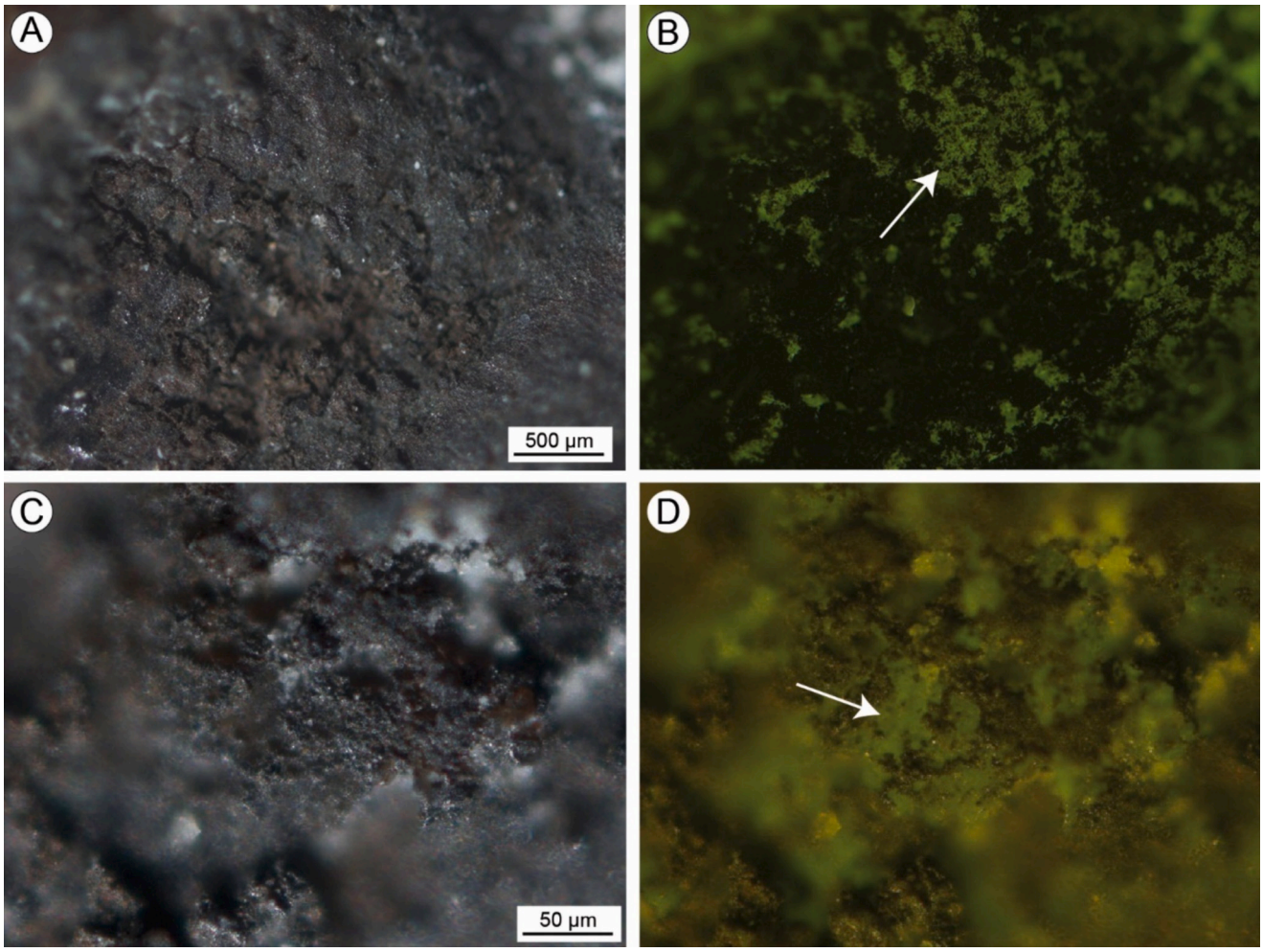

Fig. 4. Observations under incident light (A, C) and UV-Epifluorescence (B, D) of the dark external cover of the crust. The dark patina is formed by fine minerals organized in clots and amorphous material. Observation under UV-light (B, D) shows bright fluorescence of the amorphous material mixed with the fine dark minerals (white arrows). B was acquired only under UV-excitation, whereas D was acquired with both incident light and UV-epifluorescence to highlight the distribution of amorphous organic material among the fine minerals.

recognized by XRPD analyses (Fig. 8). Al and Si, detected in the external part of the crusts, could be due to detrital clay minerals that were not revealed by XRPD analyses.

EDS mapping was used to detect the distribution of the main elements within the crusts. Manganese (Mn) and iron (Fe) are concentrated on the black external patina that covers the crusts. In contrast, the thicker inner part shows a high concentration of calcium (Ca) and phosphorous (P), followed by fluorine (F), sodium (Na) and sulfur (S) (Fig. 8).

Point analyses and transects, from top to bottom of the crusts, performed by EDS allowed detection of the concentrations of the main elements in the francolite crusts. Ca and P show comparable concentration (~69 wt% and 26 wt% respectively) independent of position in the crusts, whereas F shows a clear decrease in concentration (from ~5 to ~1 wt%) from the top to the bottom of the crusts.

The homogeneous composition of the internal part suggests that variations in color and degree of cementation are not linked to mineralogy, but possibly to differing degrees of diagenetic preservation. Decreasing concentration of F (Fig. 8), and the porous and powdery characteristics of the older part of the crust (white portions), are probably linked to deterioration during ageing. This may also account for decoloration of the apatite crust.

The analyses were also used to detect specific mineral phases associated with putative bacterial remains. Most of the filaments, showing transverse segmentation and longitudinal streaks, or encrusted by fine anhedral minerals, have a francolite-like composition, whereas the walls of the coccoid-like corpuscle are ferromanganese. This dual mineral composition of the external patina is shown by both the EDS and EPMA analyses and reveals a minority francolite phase specifically within the main ferromanganiferous composition of the black cover.

Micro-Raman spectra establish the mineralogy of the two distinct parts of the crusts. Moreover, these analyses confirm that the bright fluorescence of ferromanganiferous oxides and francolite is due to the presence of organic matter localized in the minerals. In detail, Raman spectra reveal, beyond the typical peaks of Fe—Mn oxides (around 380 cm^{-1}, 490 cm^{-1} and 580 cm^{-1}; Fig. 9) and francolite (around 430 cm^{-1}, 590 cm^{-1}, 610 cm^{-1}, 960 cm^{-1}, 1040 cm^{-1} and 1080 cm^{-1}; Fig. 9), a distinct peak around 1600 cm^{-1}, related to the presence of G bands, and minor peaks at 1340 cm^{-1}, related to the D band (Fig. 9). These peaks, characteristics of amorphous carbon (AM), record the presence of residual organic matter. Raman spectra of the external black patina reveal weak francolite peaks, among peaks typical of Fe—Mn oxides and organic matter.

These data agree with SEM/EPMA microanalyses which indicate minor precipitation of francolite among the ferromanganiferous cover. A peak around 2100 cm^{-1} was detected on the spectra of the francolite portion. This peak is not reported in spectra stored in the database, nor as typical of francolite minerals, but the presence of this peak on the

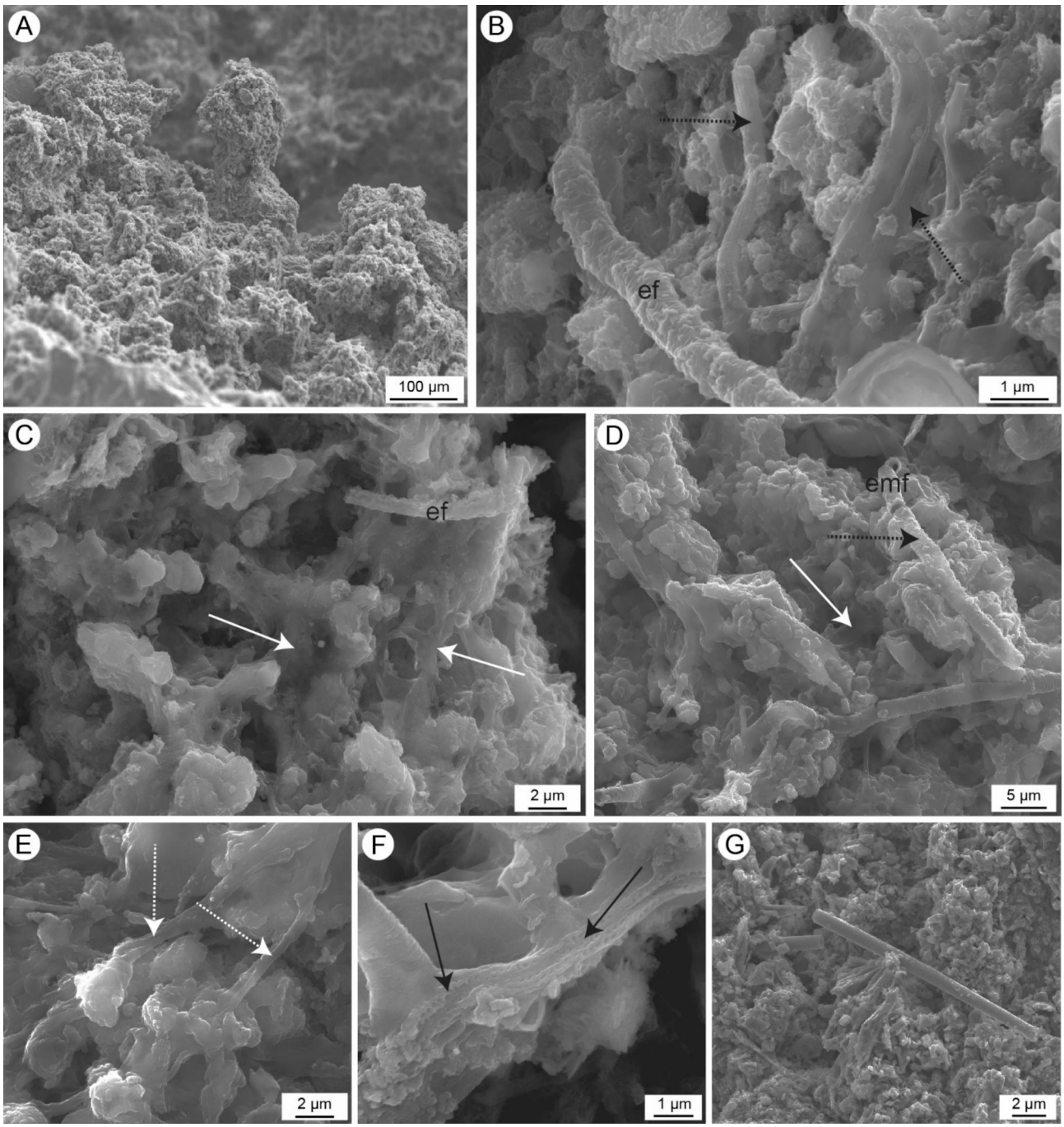

Fig. 5. SEM photos of the external dark patina covering the crusts. (A) General view of the fine minerals organized in peloidal clots. (B-F) Mineralized bacterial (and possibly fungal) filaments closely mixed with fine minerals and amorphous organic material (white arrows in C and D): the filaments show smooth (dashed white arrows in E), woven (black arrow in F) or segmented (dashed black arrows in B and D) external surface. (G) Sponge spicules on the external surface of the crusts. Note also the presence of microbial filaments encrusted by fine minerals (ef in B and C) and microbial filaments lacking external encrustation and with internal empty cavities (emf in D).

acquired spectra and the decreasing intensity from top to the bottom of the crust are consistent with decrease in fluorine, and may be related to the diagenetic evolution of the francolite.

4.3. Microorganisms involved in the biogenesis of the ferromanganiferous crusts: evidence for a "core microbiota" from comparative 16S rRNA gene metabarcoding analysis

16S rRNA gene metabarcoding data from Zinzulùsa Cave samples were previously published (Talà et al., 2021). In this study these data were compared with those made available in other studies dealing with microbial populations living on ferromanganiferous (Fe—Mn) crusts in order to identify specific microbial taxa of this type. Therefore, we selected two studies for which raw 16S rRNA gene metabarcoding data (fastq sequences) are available have been selected, so that they could be processed with the metabarcoding data of the Zinzulùsa Cave samples using the same bioinformatics pipeline (by Illumina BaseSpace pipeline and Green Genes Database), in order to reduce systemic biases during processing of the data (Nearing et al., 2021). Table S1 lists the sources of fastq sequences used for our dataset construction. Comparative analysis

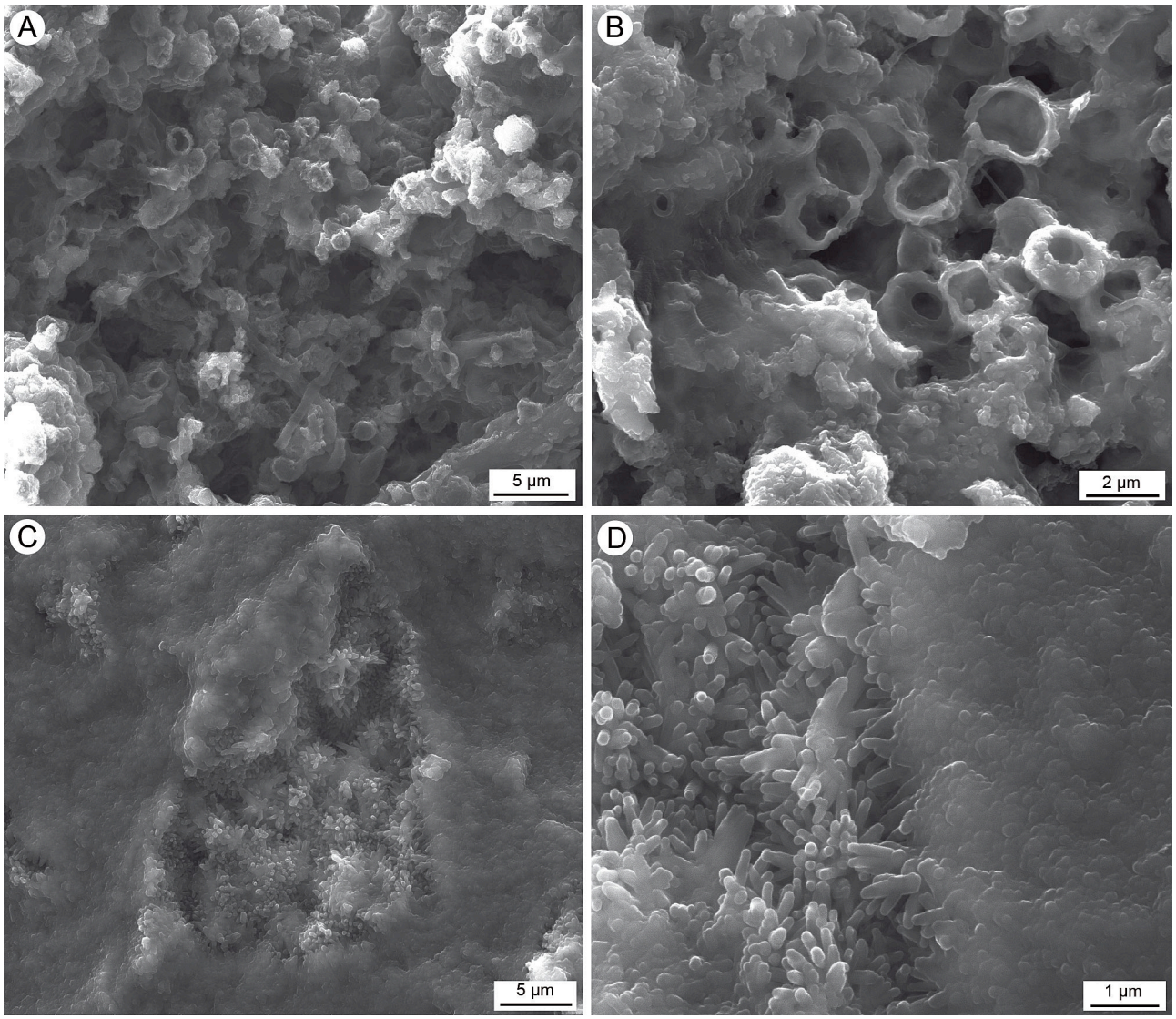

Fig. 6. (A, B) Mineralized spherulites (putative coccoid bacteria) present on the external dark surface of the crusts; note empty internal cavities of the corpuscles and nanometer size material forming the walls. (C, D) Fine minerals of the internal part of the crust; note the very fine size of the bacilli-like corpuscle.

demonstrated 133 genera or candidate genera exhibiting a relative abundance >0.1 % in at least 10 out of a total of 30 samples analyzed (Fig. S1 and Fig. S2). Within-sample relative abundance of these genera was used to generate a hierarchical clustering of samples (Fig. 10).

For the following 20 of the 133 genera or candidate genera identified, metabolic and physiological characteristics and/or the precise taxonomic collocation are not available: Gp2; Gp4; Gp6; Gp7; Gp9; Gp10; Gp13; Gp15; Gp16; Gp17; Gp21; Gp22; Gp23; BRC1 generates incertae sedis; ZB3 generates incertae sedis; Subdivision 5 generates incertae sedis; Armatimonadetes gp2; Latescibacteria genera incertae sedis; Poribacteria genera incertae sedis; Parcubacteria genera incertae sedis. The remaining 113 genera were tentatively grouped according to key metabolic and physiological characteristics. These groups included: i. nitrogen-fixing bacteria (*Bradirhyzobium, Ensifer*); ii. nitrifying bacteria (*Nitrosopumilus*, *Nitrosococcus, Nitrosospira*, *Nitrospira*); iii. sulfur/thiosulfate/sulfide-oxidizing bacteria (*Ectothiorhodospira*, *Halothiobacillus*, *Thioalkalivibrio*, *Thiocapsa*, *Thiodictyon, Thiogranum*, *Thiohalobacter*, *Thiolapillus*, *Thioprofundum*); iv. sulfate/thiosulfate/sulfur-reducing bacteria (*Brockia*, *Desulfobulbus*, *Desulfofaba, Desulfomonile*, *Desulfonatronospira*, *Desulfopila*, *Desulfosporosinus*, *Desulfotomaculum*, *Desulfovibrio*, *Dethiosulfovibrio, Thermanaerovibrio, Thermodesulfovibrio*); v. iron/sulfur-oxidizing bacteria and metal(loid)-related genera (*Acidiferrobacter*); vi. iron-oxidizing bacteria (*Ferrovibrio*); vii. iron-oxidizing and reducing bacteria (*Ferrimicrobium, Ferrithrix*); viii. iron/manganese/nitrate-reducing bacteria (*Deferribacter*, *Geobacter*; this group may also include *Carboxydocella*); ix. methanotrophic bacteria (*Methylobacter*, *Methylobacterium, Methyloceanibacter, Methyloligella*, *Methylomonas*, *Methylosinus*); x. stalked, budding Hyphomicrobiaceae (*Afifella*, *Filomicrobium, Hyphomicrobium*, *Pedomicrobium* - this group also includes *Methyloligella*); xi. Planctomycetes-Verrucomicrobia-Chlamydiae (PVC) group bacteria (*Blastopirellula*, *Rhodopirellula*, *Gimesia*, *Phycisphaera*); xii. fruiting body-forming and gliding bacteria (*Anaeromyxobacter, Enhygromyxa*, *Haliangium*, *Phaselicystis*, *Polyangium*); xiii. polyphosphate-accumulating bacteria (*Gemmatimonas*, *Congregibacter*); xiv. obligately intracellular bacteria (*Ehrlichia*, *Coxiella*); xv. obligately syntrophic bacteria associated with hydrogenotrophic methanogens (*Syntrophorhabdus*); xvi. heterotrophic fermentative bacteria (*Carboxydocella*, *Clostridium*, *Caldanaerobacter*, *Lactobacillus*, *Propionibacterium*, *Corynebacterium*, *Agrococcus*, *Brevibacterium*, *Fervidobacterium*, *Brachyspira*); xvii. Heterotrophic non-fermentative bacteria that can be distinguished based on their taxonomic classification.

Among the heterotrophic fermentative bacteria, relevant genera for the biogenesis of the Fe—Mn crusts can be represented by

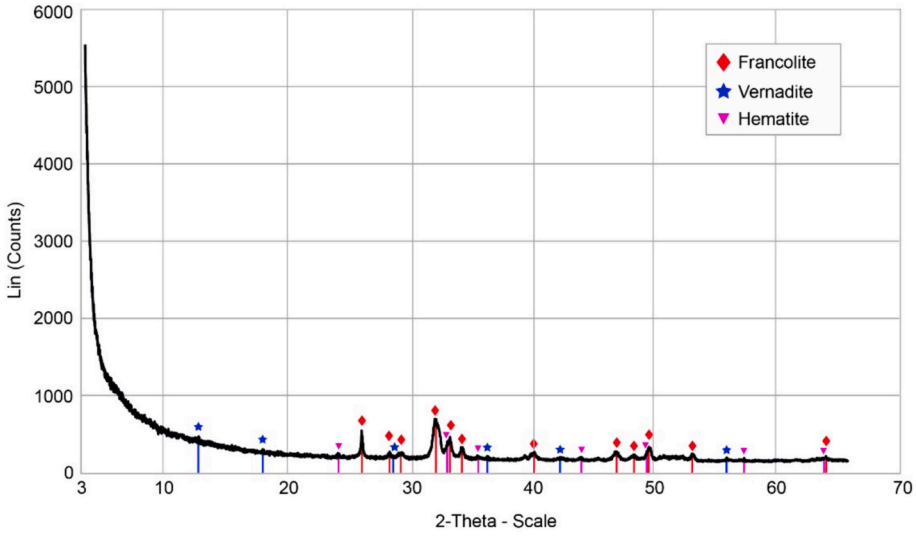

Fig. 7. X-ray diffraction patterns of the whole-powder of a representative analyzed crust sample. The main reflections of francolite, vernadite and hematite are indicated.

Carboxydocella (in particular, *Carboxidocella manganica* is a thermophilic, dissimilatory Mn(IV)- and Fe(III)-reducing bacterium) and *Brevibacterium* (manganese-solubilizing bacterium). In contrast, in the group of heterotrophic non-fermentative bacteria the presence may be noted of: (a) *Thalassobaculum*, a component of consortia with acetate- and hydrogen-scavenging methanogens; (b) *Melioribacter*, a facultative anaerobe growing by aerobic respiration, fermentation, or by reducing diverse electron acceptors [nitrite, Fe(III), As(V)]; (c) *Pseudomonas*, manganese-solubilizing bacterium; and (d) *Alkalilimnicola*, a facultatively anaerobic and facultatively chemoautotrophic haloalkaliphilic microorganism that is capable of growth with inorganic electron donors (arsenite, hydrogen, sulfide and thiosulfate) and nitrate as the electron acceptor.

In the group of heterotrophic non-fermentative bacteria, many genera belonging to Hyphomicrobiales and Rhodospirillales may be also noted, as well as the presence of many genera with the potential ability to degrade hydrocarbons and a variety of recalcitrant compounds, such as: a) petroleum hydrocarbon-degrading bacteria (*Marinobacter*, *Marinobacterium*, *Oceanospirillum*, *Oceanibaculum* in microbial consortia); b) carbazole-degrading bacteria (*Kordiimonas*); c) acetonitrile-degrading bacteria (*Natronocella*); d) alkylbenzenesulfonate-degrading bacteria (*Parvibaculum*); e) polyvinyl alcohol-degrading bacteria (*Povalibacter*); f) bacteria degrading naphthenic acids in microbial consortia (*Litorilinea*); g) bacteria degrading phenol, aniline, nitrobenzene, phenanthrene (*Novosphingobium*).

4.4. Microorganisms involved in the biogenesis of the ferromanganiferous crusts: evidence for specific manganese-metabolizing bacterial taxa by Python-based analysis of 16S rRNA gene metabarcoding data

It has been recently shown that Mn(II) oxidation in the presence of oxygen may provide energy to microorganisms (LaRowe et al., 2021), and a new candidate species has been described, "*Candidatus* Manganitrophus noduliformis", which is able to couple extracellular Mn(II) oxidation to aerobic energy conservation and CO_2 fixation by the reverse tricarboxylic acid cycle (Yu and Leadbetter, 2020; Yu et al., 2022). As Mn(II)-oxidizing chemolithoautotropy may well support biogenesis of Fe—Mn crusts, the presence of this novel taxon was investigated in the 16S rRNA gene metabarcoding dataset of the Zinzulùsa Cave samples.

16S rRNA gene sequences are available of several "*Candidatus* Manganitrophus" strains, including "*Ca.* Manganitrophus noduliformis" HYJII51-Mn-bac16s-1-B09, "*Ca.* Manganitrophus sp." isolates GAC1 and GAC2, and clones HM187074 and EU491114. In the V3-V4 region of the 16S rRNA gene, the percent identity between the sequence of "Ca. Manganitrophus noduliformis" HYJII51-Mn-bac16s-1-B09 and the other sequences ranges between 92.06 % and 100 %.

On the basis of this information, we searched for sequences close to those attributed to the genus "Ca. Manganitrophus" in the 16S rRNA gene metabarcoding database of the Zinzulùsa cave. This approach was motivated by the fact that the description of the "*Ca.* Manganitrophus sp." is very recent, and that the 16S rRNA gene sequences of this microorganism are currently assigned to unknown genera in the databases used by Illumina BaseSpace pipeline for taxonomic classification. In this analysis we used 16S rRNA gene metabarcoding data from both the Fe—Mn crusts on the rocky wall of the cave (ZC1, ZC2, ZC3, and ZC4) and those from the sediment (ZS1, ZS2, ZS3, ZS4) (PRJNA1026609). This investigation extended the other datasets analyzed in this study (DSC-S, DSC-G, and SC).

The search was carried out using an ad hoc Python script and led to the identification of 153 sequences that showed >90 % identity with respect to "*Ca.* M. noduliformans". Similarly, 1914 and 3315 sequences were identified using the 16S rRNA gene sequences of "*Ca.* Manganitrophus sp." isolates GAC1 and GAC2 as input, respectively (Tables S2 and S3). These sequences were compiled into a single file, and duplicated sequences were removed, resulting in a file containing 1954 unique sequences (Table S3). These sequences were used as input for a second ad hoc Python script with the aim of calculating the identity between the 1954 unique sequences and 9 reference sequences of "*Ca.* Manganitrophus spp." (Manganitrophus_references fasta files; DOI: https://doi.org/10.5281/zenodo.10575873). The reference sequences included "*Ca.* Manganitrophus noduliformis" HYJII51-Mn-bac16s-1-B09, "*Ca.* Manganitrophus sp." isolates GAC1 and GAC2, and 6 other sequences form EzBioCloud database (HM187074, GQ402794, GQ342365, EU491114, AY734241, and AY734239).

Sequences with >95 % identity were selected and subsequently submitted to the EzBioCloud 16S rRNA gene-based identification tool (Yoon et al., 2017) for taxonomic assignment. Furthermore, since the genus "Ca. Manganitrophus" is phylogenetically included in the class "Ca. Trogoglia", a second threshold was used, i.e., sequences with identity >91 %, to search for bacteria belonging to this class using the same EzBioCloud 16S rRNA gene-based identification tool.

In total, 125 sequences were provisionally assigned to the genus "Ca. Manganitrophus" or to the class "Ca. Trogoglia" (Table S4; Manganitrophus_ZS.fasta; DOI:https://doi.org/10.5281/zenodo.10575873).